INTERFERENCE REFLECTION MICROSCOPY

A Quantitative Theory for Image Interpretation and its Application to Cell-Substratum Separation Measurement

David Gingell and Ian Todd, *Department of Biology as Applied to Medicine, The Middlesex Hospital Medical School, London W1P 6DB, England*

ABSTRACT We propose a quantitative theory of microscope interferometry where the specimen is illuminated by a cone of monochromatic light of solid angle 0–100°, corresponding to an illuminating numerical aperture of 0 to ~1.2. Computed results compare favorably with photometric measurements of fringe irradiance for a water wedge 0–2,000-nm thick. The interpretation of cell-substratum interference images is discussed in relation to the theory. We conclude that in assessing cell-glass separation, the cytoplasmic thickness does in general contribute significantly to the final image, but this contribution is minimized at high illuminating apertures. In these circumstances, however, normal incidence theory is inapplicable and the theory for finite illuminating aperture is essential. Neglect of this fact can lead to errors of up to 100% in estimated cell-glass separation.

INTRODUCTION

Estimation of cell to substratum separation by using epi-illumination microscope interferometry is a relatively new technique in which there is currently much interest. Since the pioneering cell biological application by Curtis (1), high quality equipment has become available from Carl Zeiss (Oberkochen, West Germany) and other manufacturers. The technique has been used for the study of fibroblast-glass contact during cell locomotion (2–4), and also in analyzing the mechanism of release of cells from adhesion to glass by proteolytic enzymes and chelating agents (5). The same method has been used to examine the closeness of contact between amoeboid *Naegleria* and glass over a range of salt concentrations (6). We have carried out extensive quantitative studies on red-cell adhesion to defined interfaces (7) and have obtained interferometric evidence of a secondary minimum gap, indicating adhesion due to the balance of electrostatic and electrodynamic forces (8). White light interferometry, which is commonly employed in cell biological studies, is useful because it can give information about the order of interference fringes; the zero-order fringe colors are unmistakable and can be used as a reference for counting subsequent fringes. The first-order colors are similarly distinctive. Despite the availability of interference color charts (Carl Zeiss; S41-500.0 e), the subjective nature of color recognition reduces the use of white light interferometry to a semiquantitative level, and the alternative approach, used in precision interferometry, is to employ monochromatic light. The optical path through a thin film can be calculated from the photometrically measured film irradiance in relation to some convenient background irradiance by using normal incidence theory. However, in microscope interferometry, much of the illuminating light strikes the object at large angles (up to 50° to the normal) and despite its

wide use, the extent to which normal incidence theory can be applied has never been resolved. The problem can to some extent be circumvented by using a small illuminating aperture (1) at the expense of reduced image radiance. Izzard and Lochner (3) made a qualitative appraisal of the effect of angle of incidence on image contrast in a study of cell-substratum contact and came to the interesting conclusion that large illuminating aperture destroyed the contribution to the image derived from relatively thick layer of cytoplasm while preserving the image due to a thin film of water between cell and glass. This raises the further question of whether Curtis's results (1) obtained at low illuminating aperture included complicating contributions from the thick layer of cytoplasm. It suggested to us that a quantitative treatment of illumination at finite apertures would make it possible to measure cell-substratum gaps in monochromatic light at large illuminating aperture with minimal cytoplasmic artefact. We describe a theory of interference image intensity for a cone of incident light having a maximum angle of up to 50° to the normal (illuminating numerical aperture, INA = 1.20). This theory has been assessed in relation to measurements on a thin film of water sandwiched between glass coverslips. We shall finally discuss the results in relation to cell-substratum separation, using a multilayer model.

CALCULATION OF INTERFERENCE FOR A MULTIPLE THIN FILM

We have used a multilayer model because of its appropriateness for describing cell-substratum adhesion. For calculating (glass/water/glass) interference, which we also measured, the multilayer was reduced to a single film. We consider monochromatic light incident on the multilayer at an angle $\theta_1(n)$ (Fig. 1).

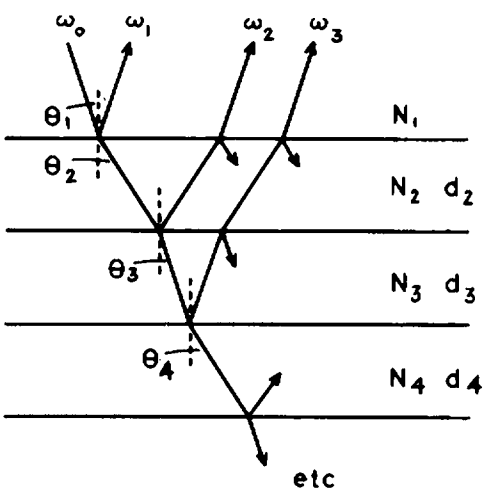

FIGURE 1 Schematic diagram showing reflection and refraction in a multilayer having refractive indices N_r and thicknesses d_r. Waves ω_r resulting from incident illumination at one angle $\theta_1(n)$ are shown. In general, the angle of refraction in layer N_r is θ_r. The value of n ranges from $n = 1, 2, 3$, up to a maximum given by $n = \Omega/\delta\theta$, where Ω is the maximum angle of incidence and $\delta\theta$ is the angular increment used in computation. Second reflections are neglected because Fresnel coefficients are small in the cases considered.

Phase differences, φ, between reflected waves, ω_r, are

$$\varphi_1(n) = \varphi_0(n) \qquad \text{where } N_1 > N_2 \tag{1}$$

$$\varphi_r(n) - \varphi_{r-1}(n) = \frac{4\pi}{\lambda} N_r d_r \cos\theta_r(n)$$

where θ_r is the angle of refraction for light of wavelength λ in a medium of refractive index, N_r, and thickness d_r.

From this we obtain phases in medium N_1 with respect to $\varphi_1(n)$

$$\varphi_r(n) = \frac{4\pi}{\lambda} \sum_{2}^{r} N_r d_r \cos\theta_r(n). \tag{2}$$

π must be added to the reflected phase whenever light passes from medium N_r to medium $N_{r\pm1}$ where $N_{r\pm1} > N_r$.

Putting I_I = incident irradiance, I_R = reflected irrandiance, I_T = transmitted irradiance, we write for perpendicular (s) components

$$I_R^S(n) = I_I^S(n)\,[F^S(n)]^2 \text{ and } I_T^S(n) = \frac{\cos\theta_r}{\cos\theta_{r\pm1}}\,[I_I^S(n) - I_R^S(n)] \tag{3}$$

and for parallel (p) components

$$I_R^P(n) = I_I^P(n)\,[F^P(n)]^2 \text{ and } I_T^P(n) = \frac{\cos\theta_r}{\cos\theta_{r\pm1}}\,[I_I^P(n) - I_R^P(n)] \tag{4}$$

Values $F(n)$ represent amplitude Fresnel coefficients as a function of incident angle $\theta_1(n)$, which are expressed for parallel polarization as

$$F^P(n)_{r\to r\pm1} = \frac{N_{r\pm1}\cos\theta_r(n) - N_r\cos\theta_{r\pm1}(n)}{N_{r\pm1}\cos\theta_r(n) + N_r\cos\theta_{r\pm1}(n)}, \tag{5}$$

where $F^P(n)_{r\to r\pm1}$ represents the amplitude coefficient for light traveling from layer r to layer $r\pm1$. Angles in layers r and $r\pm1$ are $\theta_r(n)$ and $\theta_{r\pm1}(n)$, respectively. For perpendicular polarization the coefficients are given by

$$F^S(n)_{r\to r\pm1} = \frac{N_r\cos\theta_r(n) - N_{r\pm1}\cos\theta_{r\pm1}(n)}{N_r\cos\theta_r(n) + N_{r\pm1}\cos\theta_{r\pm1}(n)}. \tag{6}$$

From Snell's law,

$$\theta_{r\pm1}(n) = \sin^{-1}\left[\frac{N_r}{N_{r\pm1}}\sin\theta_r(n)\right]. \tag{7}$$

The first state of the computation consists of forming the vector sum for all waves in medium N_1 that have been reflected from the different interfaces of the multilayer. This is done for all angles of incidence $\theta_1(n)$ on the N_1/N_2 interface; the vector components thus obtained are summed to give the final irradiance. To take into account the fact that relatively more light reaches the focus of the objective from larger angles, and also to convert from a two-dimensional distribution to a cone of incident light, it is necessary to weight each incident wave by a function of angle $W^2(n)$ for each $\theta_1(n)$. The derivation of this function will be discussed below. As W^2 is defined as an irradiance (I) weight function and $I \propto a^2$, where a = amplitude, we have for the waves shown in Fig. 1,

$$\omega_r = W(n)\,\bar{a}_r(n)e^{i\varphi_r(n)}, \tag{8}$$

where $\bar{a}_r \equiv a_r e^{i\omega t}$ is the complex amplitude.

The vector sum for the waves in medium N_1 for *one* incident angle $\theta_1(n)$ is therefore

$$\sum_r W(n)\bar{a}_r(n)e^{i\varphi_r(n)} = W(n)\bar{a}_F(n)e^{i\varphi_F(n)}, \tag{9}$$

where $\bar{a}_F(n)$ and $\varphi_F(n)$ represent the amplitude and phase of the resultant wave. We now have to sum these resultants over the angle due to the finite illuminating aperture. This is in reality a continuous process, whereas computation requires it to be broken down into a sum over n discrete angular components. The angular increment used in computation is $\delta\,\theta$ such that $n = \Omega\,/\,\delta\,\theta$, where Ω is the maximum angle (determining the illuminating numerical aperture, INA $= N_1 \sin \Omega$).

There are two distinct ways in which the components $\{W(n)\bar{a}_F(n)e^{i\varphi_F(n)}\}$ can be summed over all $\{\theta_1(n)\}$ according to whether the light striking the film system at different angles is considered to share a common phase (coherent) or not (noncoherent). We have performed calculations according to both models. For noncoherent light, we sum the squared amplitudes (giving energy, or irradiance) obtained by multiplying each complex wave by its complex conjugate.

$$I_{NC} = \sum_{n=1}^{\Omega/\delta\theta} [W(n)\bar{a}_F(n)e^{i\varphi_F(n)}][W(n)\bar{a}_F^*(n)e^{-i\varphi_F(n)}]. \tag{10}$$

In contrast, with coherent light, the terms must be added vectorially, in which case the irradiance is obtained as the product of the complex sum with its complex conjugate

$$I_C = \left[\sum_{n=1}^{\Omega/\delta\theta} W(n)\bar{a}_F(n)e^{i\varphi_F(n)}\right]\left[\sum_{n=1}^{\Omega/\delta\theta} W(n)\bar{a}_F^*(n)e^{-i\varphi_F(n)}\right]. \tag{11}$$

These irradiances are expressed as ratios of that I_I from the N_1/N_2 interface alone, which is defined as a reference (where $N_2 = N_3 \ldots N_r$).

For noncoherent light,

$$I_{NC}^R = \sum_n W^2(n)\,|\,a_1(n)\,|^2, \tag{12}$$

where summation runs from $n = 1$ to $\Omega/\delta\theta$.
For coherent light,

$$I_C^B = \left[\sum_n W(n)\bar{a}_1(n)\right]\left[\sum_n W(n)\bar{a}_1^*(n)\right] = \left[\sum_n W(n)\,|\,a_1(n)\,|\right]^2. \tag{13}$$

These summations are performed separately for perpendicular (s) and paralled (p) components of the incident light because they do not interfere. The final irradiance ratios computed are therefore, for coherent light,

$$[I_C(s) + I_C(p)]/[I_C^B(s) + I_C^B(p)], \tag{14}$$

and for noncoherent light,

$$[I_{NC}(s) + I_{NC}(p)]/[I_{NC}^B(s) + I_{NC}^B(p)]. \tag{15}$$

It is important, especially in the case of coherent illumination, that the stepsize $\delta\theta$ is sufficiently small; if it is too large, the situation can arise wherein vector quantities are added at angles $\sim\pi$, which after several iterations gives nonsense. Our approach was empirical: we progressively reduced $\delta\theta$ until further reductions caused an acceptably small change ($< 1\%$) in computed flux-density for the largest value of separation d_2 at maximum incidence, Ω. This necessitated setting $\delta\theta = 0.001$ rad for the larger apertures, where optical path lengths and consequently phase angles $\varphi_F(n)$ change rapidly with $\theta(n)$. With such a small stepsize, the calculation of intensities for $\Omega = 0.91$ rad (52°; Table I) at 10-nm intervals up to $d_2 = 1{,}000$ nm requires almost 10^6 vector additions. This extensive arithmetic was performed with tolerable running times on the CDC computer (Control Data Corp., Minneapolis, Minn.) at Imperial College, London.

TABLE I
MEASUREMENT OF INA

Aperture diameter	INA Equivalent angle Ω in degrees shown					
	Visual*	Visual‡	Photometric measurement of angular irradiance			
			Outer limit of detectable light		Mean value from sigmoid region	
mm		Field open	Field open	Field shut	Field open	Field shut
0.5	0.45	0.45	0.47 (17°)	0.45 (17°)	0.33 (13°)	0.33 (13°)
1.0	0.84	0.80	~0.76 (30°)	~0.69 (27°)	0.57 (22°)	0.62 (24°)
1.5	1.07	1.04	~0.96 (39°)	~0.91 (37°)	0.85 (34°)	0.87 (35°)
2.0	—	—	~1.20 (52°)	~1.18 (51°)	~1.15 (49°)	~1.15 (49°)

*Izzard and Lochner (3).
‡Our method.

METHOD OF INTERFEROMETRIC MEASUREMENT

A Zeiss Universal R microscope was used with Zeiss epi-illuminator type IIC (Carl Zeiss). One ocular of the binocular head was used for photometry. A 300-μm diameter pinhole with x-y adjustment was mounted at the aerial image plane and light that passed through it was scattered by a glass diffuser before entering an Oriel 3060 photomultiplier (PM) (Oriel Corp. of America, Stamford, Conn.). A light tight shutter was located between pinhole and diffuser. With a X-100 planachromat objective and X-1.5 magnification in the microscope tube the object diameter imaged at the pinhole was $300/150 = 2$ μm. The pinhole was adjusted so that it was centered on a point in the object plane that was also located by a cross hair graticule in the other ocular of the binocular head. This made it possible to measure irradiance over defined localized areas. High voltage to the PM tube was obtained from an EMI photomultiplier supply (EMI Electronics Ltd., Ruislip, England) and the signal from the tube was fed by triaxial low noise cable to a Keithley model 616 digital electrometer (Keithley Instruments, Inc., Cleveland, Ohio), whose output was used to drive a pen recorder. The light source was an Oriel (Oriel Corp. of America) ozone-free 1-Kw Xenon arc. A system of supplementary lenses in addition to the standard lamp condenser provided a suitable compromise between maximizing irradiance and minimizing the size of the arc's image at the lamp aperture diaphragm, for Kohler illumination. Adequate heat removal from the beam was achieved with some difficulty. We used a flow chamber with optically flat windows through which bubble-free water at 30°C was passed by a Zeiss thermostatted pump (Carl Zeiss). We did not use tap water because air bubbles caused serious image flickering; furthermore, if the water is too cold, condensation occurs on the chamber windows. The chamber had a silica window near the lamp, while the further window was cut from a heat absorption filter. A Leitz heat reflection filter (E. Leitz, Wetzlar, West Germany) and a further infrared absorption filter were placed in the light path after the water chamber. A Zeiss interference filter (Carl Zeiss), transmitting light of wavelength 5460 Å followed the heat filters.

An interference object in the form of a water wedge was prepared by firmly pressing a few microliters of double distilled water between Chance #1 microscope coverslips (Chance Propper Ltd., Smethwick, Warley, England) temporarily supported on a glass block. Glass was cleaned in nitric acid/hydrofluoric acid, and then well rinsed in double distilled water, and dried. The edges of the coverslip preparations were oiled to prevent evaporation, with ensuing changes in the interference pattern. Unwanted interfaces were obviated by oiling the microscope lens to the thin film preparation and by bringing the lower surface of the coverslip preparation into contact with an optical sink, consisting of a reservoir of Zeiss immersion oil (Carl Zeiss) with dissolved Sudan black dye. Background irradiances were measured by using a clean glass coverslip oiled to the objective lens: the other side of the coverslip was brought into contact with distilled water in a glass vial that was matt black inside. Light scattered within the microscope at each lamp aperture setting was measured on the PM tube with the objective directly immersed in a reservoir of lens oil containing dissolved Sudan black. This, together with PM tube shot noise measured with the PM shutter closed, was subtracted from all experimental measurements, which were made in a darkened room.

MEASUREMENT OF THE ANGULAR IRRADIANCE FROM THE MICROSCOPE OBJECTIVE

Irradiance as a function of incident angle was measured by using a linear light sensitive diode (LSD) (Radiospares, no. 305–462; RS Components Ltd., London, England) fixed to a glass slide located 1.46 cm below the objective (Fig. 2). The diode was encapsulated in Hysol OSO-100 optoelectronic resin (Patent Chemicals, Inc., Paterson, N.J.), which was then carefully ground down almost to the silicon surface. A thin black mask was painted over the photosensitive region, leaving an area of ~ 0.5 mm^2 untouched. This provided a small aperture whose effective measuring area remained constant as the angle of illumination was varied. The maximum angle subtended at the focal point by the 0.5-mm aperture was 2.0°. The slide was enclosed in a blackened box filled to the level of the objective lens with immersion oil and mounted on the microscope stage so that the diode could be moved in a plane perpendicular to the optic axis at a distance h from the focal plane (Fig. 3). The diode was reverse-biased

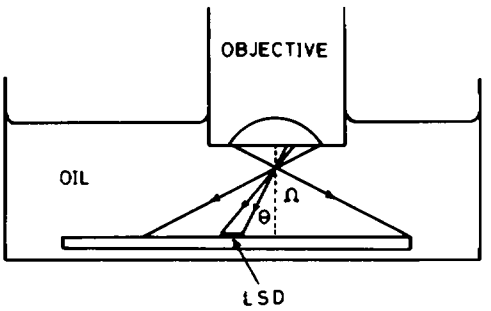

FIGURE 2

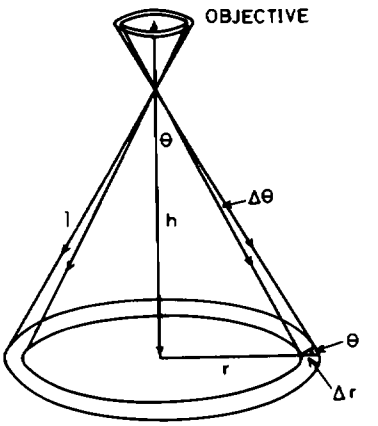

FIGURE 3

FIGURE 2 Measurement of irradiance $I(\theta)$, where θ is the incident angle. The sensitive area of the LSD subtends an angle, θ, at the focus. The diode is moved in a direction perpendicular to the optic axis to measure $I(\theta)$, up to the limiting angle Ω. Electrical connections are not shown.

FIGURE 3 Construction for calculating weight function $W^2(\theta)$ from the angular irradiance $I(\theta)$. See text for details.

and leakage current (proportional to irradiance) was measured by using a Keithley model 616 electrometer (Keithley Instruments, Inc.) whose output drove a pen recorder. Measurements were made at 1-mm steps along a line passing through the optic axis across the complete diametric field of illumination. Averaging the values at corresponding distances, r, either side of the optic axis gave a mean radial irradiance distribution that was expressed as a function of incident angle $I(\theta)$, where $\theta = \tan^{-1}(r/h)$. Angular irradiance was measured for 0.5- , 1.0- , 1.5- , and 2.0-mm lamp aperture stops. Pinholes were used in preference to an iris to give accurately defined stop positions. Because the aperture stop is in focus at the pupil of the objective, it controls the INA, which is related to the angle of the cone of light by which the objective illuminates the focal area: INA $= N_1 \sin \Omega$. For each aperture stop we used two field stop positions, either fully closed (1-mm Diam) or open to the edge of the visual field (5 mm Diam).

Results are shown in Fig. 4. The curves (normalized to a constant maximum irradiance at $\theta = 0$) follow a common $\cos^5 \theta$ law, but break away at different values of θ corresponding to the edge of the field for each aperture. Calculation of the Airey disk diameter shows that the sigmoid edge effect is about 100 × too large to be attributable to Fraunhofer diffraction. Its width is sensitive to the field iris setting but it does not appear to be simply due to the smearing of the edge, which would be caused by a finite field iris, as this is equal to the diameter of the field iris image at the focus, a maximum of 5 mm/30 for our system. This is also too small to explain the edge effect. A contributing factor may perhaps be light adventitiously reflected within the microscope..

In Table I we compared values obtained by Izzard and Lochner (3) with our photometric results. We also estimated illuminating numerical aperture by using a "direct" method. This involved adjusting the Zeiss aperture iris diaphragm (Carl Zeiss) in the condenser such that its image in the pupil of the objective coincided with one of the two extreme settings of the lens iris which is in focus at the same plane and is calibrated by Zeiss at NA = 0.8 and 1.24. From these, other values were calculated. It can be seen that the INA values estimated by methods based on visual assessment of the edge of a circle of light (our direct method and Izzard and Lochner's method) correspond approximately with the photometrically measured limit at which light is detectable, which can be estimated to about 1.5° from the graph. If the angular distribution for an ideal point source is obtained empirically by taking values of Ω corresponding to the inflexion points on the curves, we obtain estimates of the mean values of INA, with field iris open and closed, shown in Table I; this shows that INA is largely dependent on a

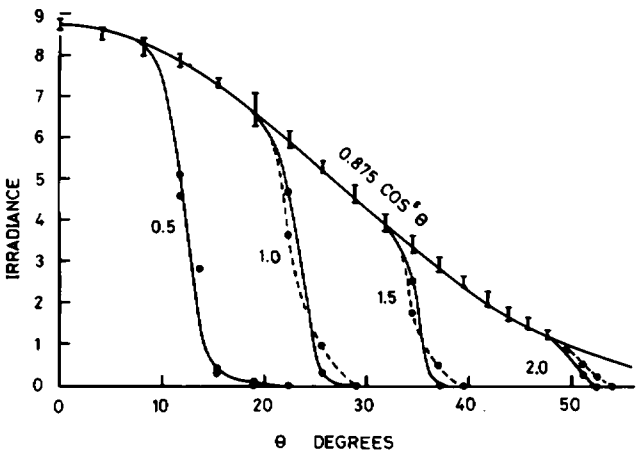

FIGURE 4 Irradiance $I(\theta)$, where θ is the incident angle, for illuminating apertures of 0.5, 1.0, 1.5, and 2.0 mm. Results for each aperture are shown for two positions of the field iris:------fully closed;——partly open. The curve $0.875 \times \cos^5 \theta$ is superimposed on the experimental points common to all aperture positions. Vertical bars include all experimental points (two sets per aperture value) except where curves depart from $0.875 \times \cos^5 \theta$, in which case individual points are plotted.

somewhat arbitrary choice of Ω. These values differ significantly from the visual estimates. It is also clear from our results that for careful work the position of the field iris must be controlled, because it has a small effect on Ω.

CALCULATION OF WEIGHT FUNCTION FROM THE IRRADIANCE

It is necessary to calculate the relative contributions to the final image irradiance that result from light impinging on the thin film at a series of angles $\{\theta_1 \ (n)\}$. This involves understanding how irradiance as a function of planar angle θ can be used to obtain the angular flux distribution for a conical shell of incident light. Let light from the objective (Fig. 3) be brought to a point focus and then strike a perpendicular plane at a distance h from the focus. Consider a ray at angle θ to the normal, and let us calculate the fraction of light which strikes the plane for a small increment $\Delta\theta$. The experimentally determined angular irradiance distribution gives the number of photons/unit area/second striking the plane as a function of θ as $AI(\theta)$ where A is a constant. Therefore the number/second striking the thin annulus swept out by $\Delta\theta$ is

$$N(\theta) = 2\pi r \, \Delta r \, AI(\theta), \tag{16}$$

because

$$\Delta r = l\Delta\theta/\cos\theta$$

and

$$l = h/\cos\theta$$

and

$$r = h/\tan\theta,$$

then

$$N(\theta) = 2\pi\, \Delta\theta h \sin\theta .\, AI(\theta)/\cos^3\theta. \tag{17}$$

Over the regions where the angular irradiance is given by $I(\theta) \propto \cos^5\theta$,

$$N(\theta) \propto \sin\theta \cos^2\theta = W^2(\theta). \tag{18}$$

Because the cone above the focus is geometrically similar to that below it, $N(\theta)$ is also proportional to the number of photons per second directed towards the focal plane from a solid conical shell of angle $\Delta\theta$ at any angle θ. Weight functions $W^2(\theta)$ for the apertures used are given in Fig. 5 and the empirical functions describing the curves are shown in Table II.

The problem has so far been treated as if light is brought to a point focus by the objective. In Kohler illumination a finite field iris is imaged at the focal plane of the objective, so we should consider what effect this may have on our calculations. If we replace the focal point (Fig. 3) by an image of the field iris subtending an angle, α, at radius, r, we can calculate the maximal value of α for our system. This occurs at $\theta = 0$ for the larger field iris of 5-mm Diam, when α is found to be 1°, which is less than the angular resolution obtainable with the LSD, so we conclude that our calculation of weight function is not appreciably in error.

INTERPRETATION OF MEASURED IRRADIANCES

Normal incidence results in symmetrical interference fringes that do not decrement with film thickness. Illumination at increasing aperture results in more and more strongly damped maxima and minima (Fig. 6). The loci of maxima and minima computed according to the noncoherent illumination model are plotted in Fig. 7, together with experimentally measured extrema for 0.5-, 1.0-, 1.5-, and 2.0-mm apertures, giving remarkable fits for most of the conditions investigated. In Fig. 8 the computed values for 1.5 mm from Fig. 7 are shown,

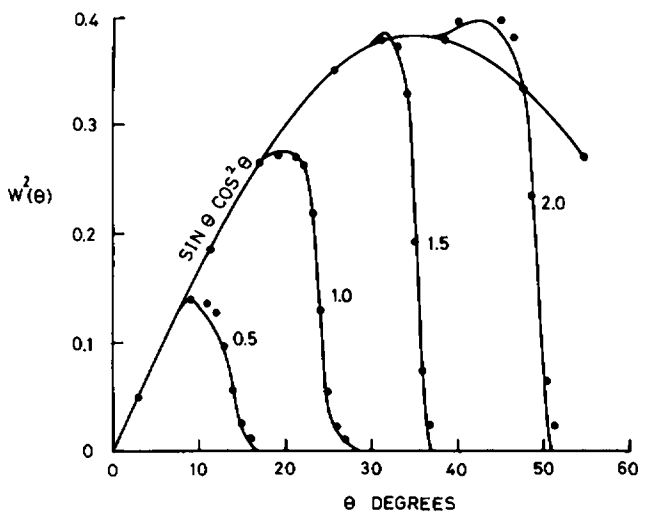

FIGURE 5 Weight function $W^2(\theta)$. Curves as in Fig. 3. Points indicate the fit of the equations given in Table II.

TABLE II
IRRADIANCE WEIGHT FUNCTIONS

Aperture diameter	Function range	Function (θ in degrees)
mm	*degrees*	
0.5	$9 \geq \theta > 0$	$\sin\theta\cos^2\theta$
	$16 > \theta > 9$	$a_1[a_2 + (\theta + a_3)^6]^{-1}$
1.0	$19 \geq \theta > 0$	$\sin\theta\cos^2\theta$
	$28 > \theta > 19$	$a_4[a_5 + (\theta + a_6)^7]^{-1}$
1.5	$30 \geq \theta > 0$	$\sin\theta\cos^2\theta$
	$37 > \theta > 30$	$a_7[a_8 + (\theta + a_9]^8)^{-1}$
2.0	$38.5 \geq \theta > 0$	$\sin\theta\cos^2\theta$
	$42.5 \geq \theta > 38.5$	$a_{10}[a_8 + (-a_{11} - \theta)^7]^{-1}$
	$51 > \theta > 42.5$	$a_{10}[a_8 + (\theta + a_{11})^7]^{-1}$

$a_1 = 1.35 \times 10^3$, $a_2 = 10^4$, $a_3 = -9$, $a_4 = 1.89 \times 10^4$, $a_5 = 7 \times 10^4$, $a_6 = -19$, $a_7 = 1.52 \times 10^5$, $a_8 = 4 \times 10^5$, $a_9 = -30$, $a_{10} = 1.6 \times 10^5$, and $a_{11} = -42.5$.

together with computed values for the same aperture according to the coherent model. All irradiances are calculated with respect to a background consisting of a (glass/water) interface. The clear difference in behavior according to coherent and noncoherent models and the close correlation between experiment and theory leaves no doubt that the noncoherent model is correct for our method of illumination, as would be expected.

It is of interest to consider the behavior of the two models more closely. A particularly striking difference is that while the mean value in the noncoherent case oscillates about 2.0, the coherent model predicts fringes that oscillate about 1.0. In Fig. 7 it can also be seen that the fringes are damped rapidly as the illuminating aperture increases. For example, at 2.0-mm aperture, extremum $B2$ (second bright fringe of curve D) is near 2.0, whereas at

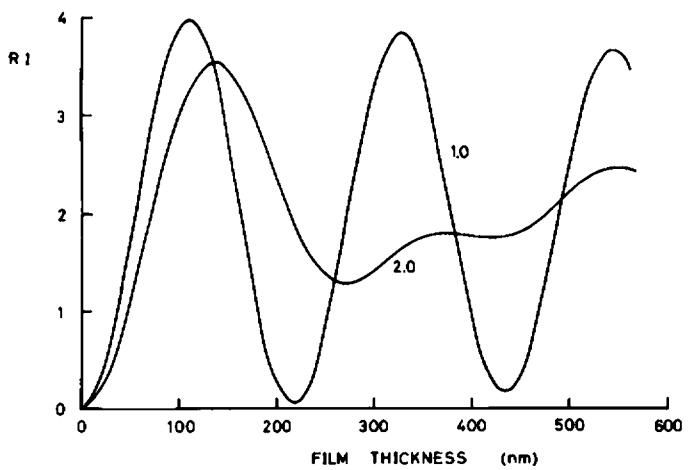

FIGURE 6 Relative irradiance RI of interference fringes (relative to background) for a thin film of water between semi-infinite glass slabs ($n = 1.52$). The first three fringes are plotted for 1.0- and 2.0-mm illuminating apertures.

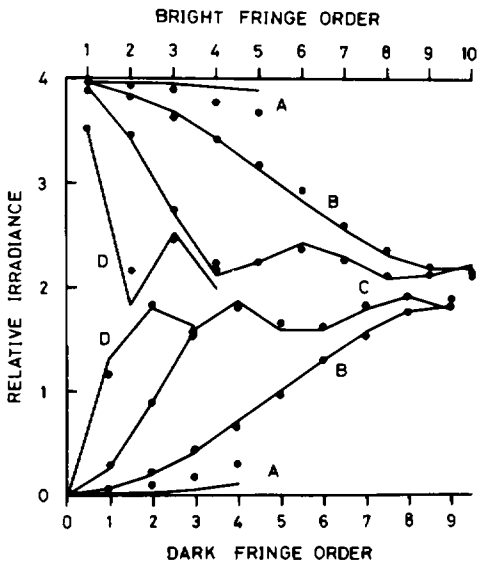

FIGURE 7

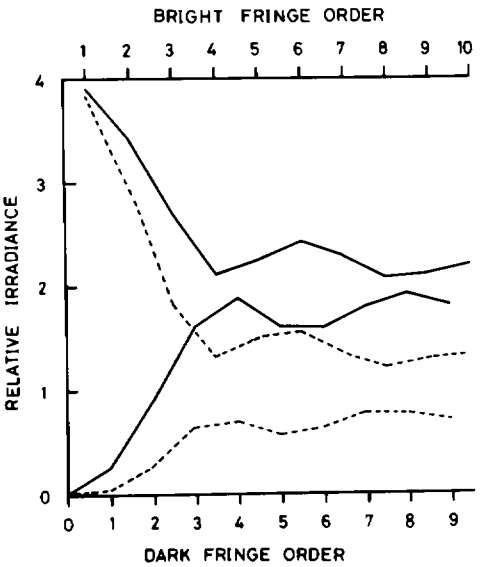

FIGURE 8

FIGURE 7 Envelopes of fringe extrema for 0.5- (A), 1.0- (B), 1.5- (C), 2.0-mm (D) illuminating apertures. Fringe *B*10 corresponds approximately to 2,000 nm. Experimental points (•) are superimposed on curves (—) calculated according to the noncoherent model. Each point is the mean of four values, except those in curves A, which represent single measurements. Prefixes *B* and *D* refer to bright and dark fringe extrema, respectively, i.e., *B*10 is the tenth bright fringe.

FIGURE 8 As in Fig. 7. Only the 1.5-mm calculated result is shown, for both noncoherent——and coherent--------models.

1.0-mm aperture the fall to 2.0 has occured only by the tenth fringe. The difference in mean value for the two models can be understood by looking at the individual interference components that result from light incident on the film at each incremental angle, Ω, from zero to the upper limit $n\delta\theta$. The multilayer system shown in Fig. 1 is reduced to a single film of water between glass, and the resultant vector from the whole film at angle of incidence $\theta_1(n)$ is

$$W(n)\bar{a}_F e^{i\varphi_F(n)} = W(n)[\bar{a}_1(n)e^{i\varphi_1(n)} + \bar{a}_2(n)e^{i\varphi_2(n)}], \tag{19}$$

where

$$\varphi_2(n) = \frac{4\pi}{\lambda} N_2 d_2 \cos\theta_2(n) + \pi \qquad (N_1 > N_2 < N_3). \tag{20}$$

For (glass/water/glass) we can put $\bar{a}_2 = \bar{a}_1$ as multiple reflections can be ignored. Writing $W(n)\bar{a}_1(n)$ as a_n and summing over all incident angles $\{\theta_1(n)\}$ we obtain the irradiance ratio (RI in Fig. 7 et seq.) for one sense of polarization of noncoherent light,

$$\frac{I_{NC}}{I_{NC}^B} = \frac{\sum_n a_n a_n^* [e^{i\varphi_1(n)} + e^{i\varphi_2(n)}][e^{-i\varphi_1(n)} + e^{-i\varphi_2(n)}]}{\sum_n a_n a_n^*} \tag{21}$$

$$= \frac{2\sum_n |a_n|^2\{1 + \cos[\varphi_1(n) - \varphi_2(n)]\}}{\sum_n |a_n|^2}, \tag{22}$$

where I^B_{NC} refers to background.
From Eqs. 1 and 20 we see that $\varphi_1(n) = 0$. Eq. 22 therefore reduces to

$$(I_{NC}/I^B_{NC}) = 2\sum_n |a_n|^2 [1 + \cos \varphi_2(n)] \Big/ \sum_n |a_n|^2. \tag{23}$$

Cos $\varphi_2(n)$ is a continuous function of n and d_2, which oscillates about a mean value of zero as d_2 increases at constant illuminating cone angle $\Omega = n\delta\theta$; similarly, as Ω increases (at constant d_2) the number of oscillations increases, so that cos $\varphi_2(n)$ oscillates about zero as either the film thickness is increased, or as the illuminating aperture is opened up. Under these conditions the mean value of the irradiance ratio approaches 2.0.

We shall now consider the mean value in the case of one sense of polarization for coherent illumination. Because the phases of all rays striking interface N_1/N_2 are in this case identical and can be set to zero, Eq. 19 becomes

$$W(n)\bar{a}_F(n)e^{i\varphi_F(n)} = W(n)[\bar{a}_1(n) + \bar{a}_2(n)e^{i\varphi_2(n)}]. \tag{24}$$

Writing $\bar{a}_1(n) = \bar{a}_2(n)$ as before; letting $W(n)\bar{a}_1(n) \equiv a_n$ and putting $\varphi_2(n) \equiv \varphi_n$,

$$\frac{I_C}{I^B_C} = \frac{\left[\sum_1^n a_n(1 + e^{i\varphi_n})\right]\left[\sum_1^n a_n^*(1 + e^{-i\varphi_n})\right]}{\sum_1^n a_n \sum_1^n a_n^*}, \tag{25}$$

which gives,

$$\frac{I_C}{I^B_C} = \frac{\left(\sum_1^n |a_n|\right)^2 + 2\sum_1^m \sum_1^{n=m} |a_m a_n| \cos \varphi_n + \sum_1^m \sum_1^{n=m} a_m a_n \cos(\varphi_m - \varphi_n)}{\left(\sum_1^n |a_n|\right)^2} \tag{26}$$

As both cosine terms again oscillate about zero, for sufficiently large n or d_2 the mean ratio is therefore 1.0.

We are thus able to account for the result that the average value of the relative irradiance is 2.0 in the noncoherent case, and 1.0 in the coherent case. Furthermore, at small distances however, Figs. 7 and 8 show that the maximum value of 4.0 is approached for both models, the closeness of approach increasing as Ω decreases, and at $d_2 = 0$ both models give zero regardless of Ω. This behavior can be rationalized by considering the equations for the relative irradiance.

When $\theta_2 = 0$ and $d_2 = \lambda/4N_2$, Eq. 20 gives $\varphi_2 = 2\pi$, so for normal incidence Eq. 23 reduces to

$$\frac{I_{NC}}{I_{NC}^{B}} = 4\frac{|a_n|^2}{|a_n|^2} = 4.0. \tag{27}$$

For any finite aperture, $\Sigma|a_n|^2 > \Sigma a_n^2 \cos\varphi_2(n)$ and $I_{NC}/I_{NC}^{B} < 4.0$.
This behavior can be seen in Fig. 7. Further, for $d_2 = 0$ (Eq. 20) the irradiance ratio (Eq. 22) goes to zero, regardless of the illuminating aperture, as required.

In the case of coherent light (Eq. 26) we have

$$\left.\begin{aligned}\varphi_n &= \frac{4\pi}{\lambda} N_2 d_2 \cos\theta_2(n) + \pi \\ \varphi_m &= \frac{4\pi}{\lambda} N_2 d_2 \cos\theta_2(m) + \pi\end{aligned}\right\}. \tag{28}$$

For $\theta_2 = 0$ and $d_2 = \lambda/4N_2$, $\cos\varphi_n = \cos(\varphi_m - \varphi_n) = 1$, so that Eq. 26 reduces to

$$\frac{I_C}{I_C^B} = \frac{\left(\sum_1^n a_n\right)^2 + 2\sum_1^m \sum_1^{n=m} a_m a_n + \sum_1^m \sum_1^{n=m} a_m a_n}{\left(\sum_1^n a_n\right)^2} = 4.0 \tag{29}$$

Again, for any finite Ω, the cosine terms in Eq. 26 result in $I_c/I_c^B < 4.0$.
In the limit $d_2 = 0$, we have $\varphi_m = \pi$ and $\varphi_m - \varphi_n = 0$, thus

$$\frac{I_C}{I_C^B} = \frac{\left(\sum_1^n a_n\right)^2 - 2\left(\sum_1^n a_n\right)^2 + \left(\sum_1^n a_n\right)^2}{\left(\sum_1^n a_n\right)^2} = 0. \tag{30}$$

The vector addition of components $W(n)\bar{a}_F(n)e^{i\varphi_F(n)}$ to form the final wave from the multilayer is conveniently illustrated in Fig. 9 for coherent illumination. The axes of the graph are the summed orthogonal components of the complex waves. The figure shows summation of the individual vectors in head-to-tail fashion for $\delta\theta = 0.05$ rad, which gives a plottable number of vectors: the resultant is obtained by drawing a straight line from the origin to the final vector component. Separate curves are shown for perpendicular (s) and parallel (p) components, which must be summed separately, as they do not interfere. The situation illustrated is a (glass/water/glass) film of thickness 1,600 mm when using an illuminating aperture of 1.5 mm, where the corresponding maximum angle of incidence $\Omega = 37°$ (Table I). A noticeable feature of the curves is the rapid attenuation of the parallel components (p) compared with the perpendicular ones (s) as the Brewster angle for the lower (water/glass) interface (41°) is approached (Fig. 1); when $\theta_1 = 37°$, $\theta_2 = 43.5°$. Net background amplitudes are represented as summed vectors of zero phase equal to $[\Sigma_n W(n)\bar{a}(n)]$ $[\Sigma_n W(n)\bar{a}^*(n)]$, which lie on the real axis; the vector sum for parallel components is B' and for perpendicular components, A'. The irradiance ratio (Eq. 14) is

$$\frac{I_C}{I_C^B} = \frac{A^2 + B^2}{(A')^2 + (B')^2} = 1.17.$$

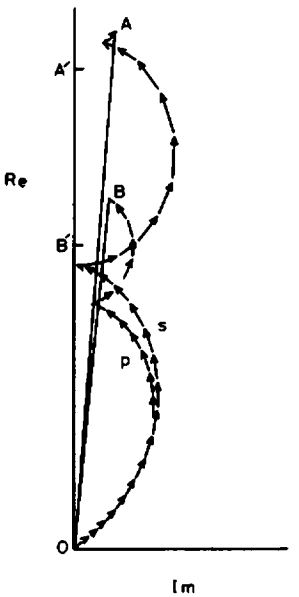

FIGURE 9 Diagram showing summation of component waves over an illuminating aperture 1.5 mm for a (glass/water/glass) film 1,600 nm thick. Parallel components *(p)*, perpendicular components *(s)*. Vectors representing the final waves from the thin film are OA and OB for the film and OA′ and OB′ for the background.

This is very close to the coherent ratio found by numerical computation for $\delta\theta = 0.001$ rad, shown in Fig. 8, where fringe *B*6 occurs near 1,600 nm. In the case of noncoherent light, the summation is conducted over the squares of the moduli of all vectors, giving an irradiance ratio of 2.0. We can appreciate a further feature of the summation shown in Fig. 9. The vectors $[W(n)\bar{a}_F(n)e^{i\varphi_F(n)}]$ form a series of arcs, showing that $\varphi_F(n)$ is a discontinuous function. Why this should be so can be seen by considering the resultant wave for one angle of incidence $\theta_1(n)$ when using Eq. 24 and setting $\bar{a}_1(n) = \bar{a}_2(n)$, $W(n)\,\bar{a}_1(n)e^{-i\omega t} = a'_n$, $W(n)\bar{a}_F(n)e^{-i\omega t} = a''_n$, $\varphi_F(n) = \varphi''_n$, $\varphi_2(n) = \varphi'_n$,

$$a''_n e^{i\varphi''_n} = a'_n(1 + e^{i\varphi'_n}) \tag{31}$$

i.e.,

$$a''_n(\cos\varphi''_n + i\sin\varphi''_n) = a'_n(1 + \cos\varphi'_n + i\sin\varphi'_n). \tag{32}$$

Equating real parts,

$$\cos\varphi''_n = \frac{a'_n}{a''_n}(1 + \cos\varphi'_n). \tag{33}$$

We have $1 \geqslant \cos\varphi'_n \geqslant -1$ and hence $2 \geqslant (1 + \cos\varphi'_n) \geqslant 0$. Because $a'_n/a''_n > 0$, $\cos\varphi''_n > 0$. Consequently, φ''_n takes only values $0 \to \pi/2$; $3\pi/2 \to 2\pi$ etc., as is the case for the phase angles of the individual vectors shown in Fig. 9.

CELL-GLASS CONTACT: A MODEL

In studying cell-glass contact, it has previously been necessary to make the normal incidence assumption (1,2). Although previous workers (3)realized that under certain circumstances a finite aperture treatment might give very different results, they did not provide a quantitative discussion of the problem. Our theory enables us to comment on their ideas, and to consider the question of whether normal incidence can be a legitimate approximation.

For modeling the cell surface, we need an estimate of the refractive index of membrane lipid. The optical refractive index of a thin lipid membrane was determined by Cherry and Chapman (9). Measurements for polarization perpendicular and parallel to the membrane gave $N = 1.486$ and $N = 1.464$, respectively. The mean value is $N = 1.475$, but for light incident at small angles the higher value may be more appropriate. Other possible values are 1.37 for n-hexane (10) and 1.41, often used as typical for hydrocarbons.

For cell membranes Wallach et al. (11) reported a refractive index of 1.56 from light-scattering measurements of membrane vesicles. This is higher than quoted values for membrane lipids and may be in error due to a lengthy extrapolation. We have used 1.45 for all calculations except those for Fig. 15, where $N_3 = N_5 = 1.50$. We appreciate that for quantitation the membrane refractive index can be critical, and also that we may have committed a serious oversimplification in assuming the membrane to be a single isotropic film. The model could easily be made more complicated, but in the absence of sufficient detailed refractive index data it would be at the expense of biological meaningfulness. The bilayer thickness is taken to be 40 Å, a value based on the x-ray result for phosphatidylcholine (12). For the refractive index of cytoplasm, phase contrast measurements on amoebae of *Dictyostelium discoideum* give 1.37.[1] In Fig. 10 we have plotted the first two fringes for normal incidence, as well as for two defined illuminating apertures. In this example, the thickness of the cytoplasm is set at 1 μm. The relationships between the curves are complicated, but it is evident that none of the finite aperture fringes corresponds even approximately to the normal incidence case. Even at 1.0-mm aperture, the error is such that a water gap of 30 nm could be construed as 90 nm. It should also be noted that for this multiple film, the irradiance ratios calculated for the smaller apertures do not necessarily correspond more closely to normal incidence than those calculated for large apertures, nor does the zero-order minimum invariably occur at zero water-film thickness. In Figs. 10, 12, and 15 we see the surprising result that as the illuminating aperture becomes finite, there is a reversal in the sign of the change in contrast with separation at small separations where significant interference effects would not have been predicted. The results, however, are quite sensitive to cytoplasmic thickness. In Fig. 11 we show corresponding fringes for a cell with only 0.5 μm of cytoplasm. Here the smaller apertures give a far better approximation to normal incidence for the first fringe, but get progressively more dissimilar as the water separation increases. Results for 3.0 μm of cytoplasm are given in Fig. 12, where it can be seen that normal incidence theory is completely inappropriate. From these comparisons we conclude that the use of normal incidence theory for assessing cell-substratum contact is strongly contra-indicated. Only for a simple thin-film at separations less than the first bright fringe would this

[1]Vince, S. Personal communication.

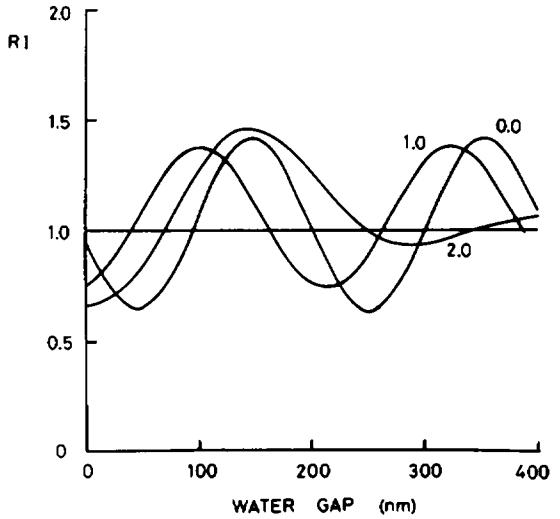

FIGURE 10 RI of interference fringes for a multilayer thin film representing cell-glass interaction. Refractive index values $N_1 = 1.52$ (glass); $N_2 = 1.33$ (water); $N_3 = 1.45$ (membrane); $N_4 = 1.37$ (cytoplasm); $N_5 = 1.45$ (membrane); $N_6 = 1.33$ (water). Lipid membrane thickness = 4 nm, cytoplasm thickness = 1.0 μm. Curves are given for normal incidence (0.0) and for illuminating apertures 1.0 and 2.0 mm. See Table 1 for corresponding angles of incidence. The abscissa is cell-glass separation (water gap).

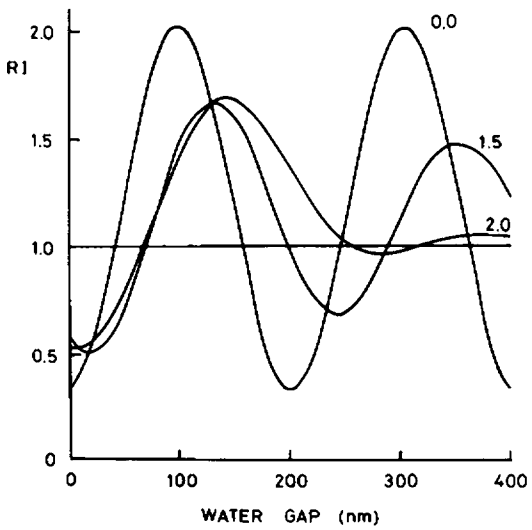

FIGURE 11

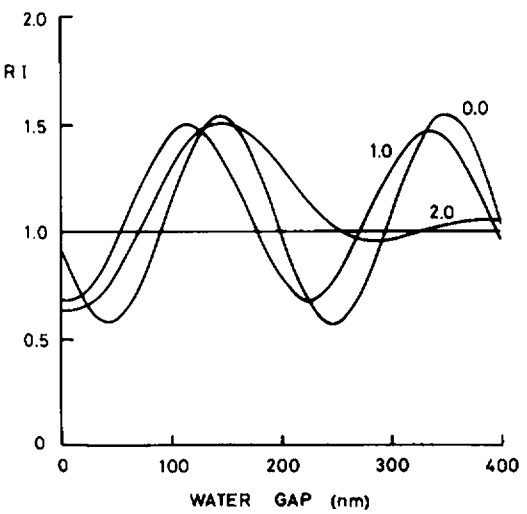

FIGURE 12

FIGURE 11 As in Fig. 10, except that the cytoplasmic thickness is 0.5 μm, and 1.5 replaces 1.0 mm aperture.

FIGURE 12 As in Fig. 10, except that the cytoplasmic thickness is 3 μm.

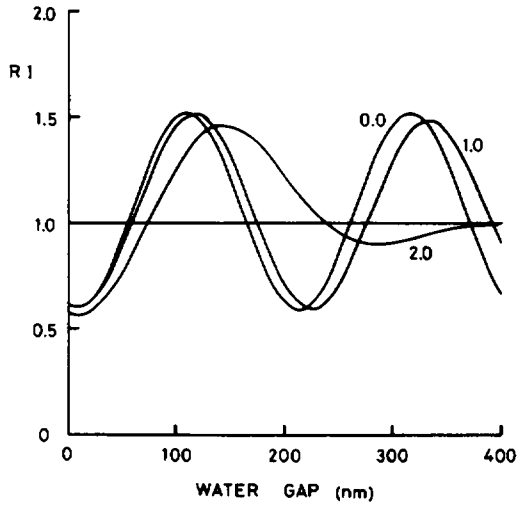

FIGURE 13 As in Fig. 10, but with infinitely thick cytoplasm.

simplification appear to be reliable (Fig. 6) and even then only by comparison with small illuminating apertures (0.5 or 1.0 mm; see Table II).

In Fig. 15 we show curves for membranes of refractive index 1.50 and 1 μm of cytoplasm for 0-, 1.0-, and 2.0-mm apertures, which should be compared with Fig. 10, where the refractive index is 1.45. It can be seen that increased refractive index increases contrast (max/min RI) as would be expected by analogy with a single film where contrast increases as

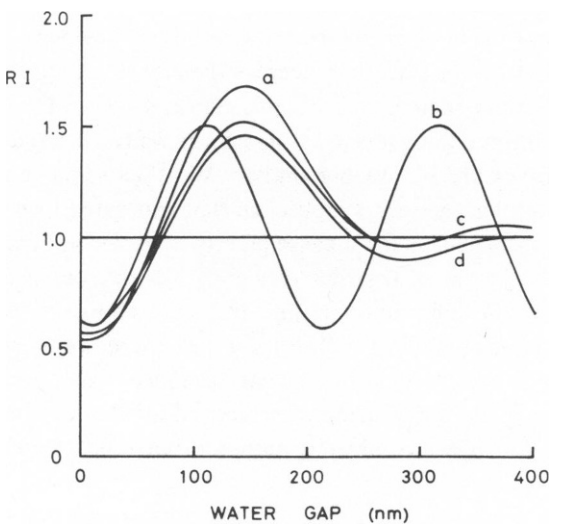

FIGURE 14 As in Fig. 10, but showing fringes for 2.0-mm illuminating aperture and cytoplasmic thickness 2.5 μm *(a)*, 0.5 μm *(c)*, and infinite cytoplasm *(d)*. Curve *(b)* shows normal incidence for infinite cytoplasm.

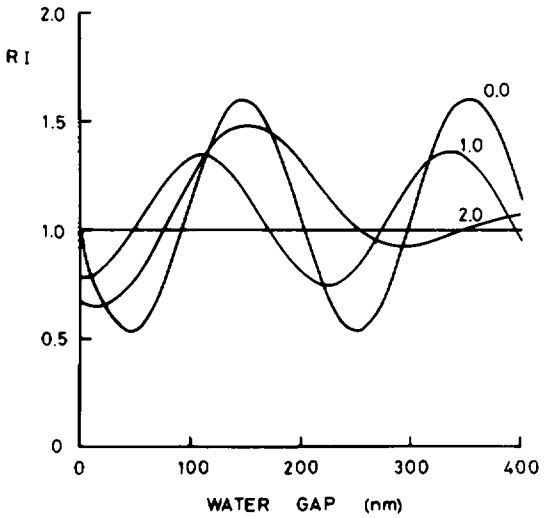

FIGURE 15 As in Fig. 10, showing fringes for normal incidence and for 1.0- and 2.0-mm apertures. Membrane refractive index ($N_3 = N_5$) increased to 1.50. Cytoplasmic thickness $d_4 = 1.0$ μm.

$N_3 \rightarrow N_1$. However, careful comparison of Figs. 10 and 15 shows that sensitivity to refractive index falls as the aperture increases, such that curves for 2.0 mm are almost identical.

A further question concerns the degree to which a thin, extended sheet of cellular cytoplasm contributes to the final interference picture.[2] The problem arises because in studying cells by interferometry, the cytoplasmic thickness is an independent variable requiring separate measurement. To investigate this problem it is necessary to compare fringes calculated for a "complete" cell, using a (glass/water/membrane/cytoplasm/membrane/water) model (Figs. 10–12) with fringes where the cytoplasm forms a semi-infinite region (Fig. 13). If Figs. 10–13 are carefully compared, it will be seen that whereas the curves are very dissimilar for smaller apertures, at 2.0-mm aperture there is considerable convergence. In Fig. 14 curves for 2.0 mm alone are plotted for an infinite thickness of cytoplasm, as well as 0.5 and 2.5 μm of cytoplasm. Above ~ 1 μm the curves are reasonably similar. We thus see a tendency for the fringe pattern for large illuminating aperture to approach that generated by a cell modeled with an infinitely thick cytoplasm, where there is consequently no reflection from the far side of the cell. This supports the suggestion of Izzard and Lochner (3) that cytoplasmic contributions to the final image are lost at high illuminating aperture. However, we must qualify our agreement: these authors imply that at high INA it may therefore be legitimate to calculate the cell-glass water gap thickness by using normal incidence theory for a single film. This is not correct. Curve *b* in Fig. 14 shows fringes for normal incidence (taken from Fig. 13) and infinite cytoplasm: it is evidently a completely inappropriate model for the high INA curves.

[2]Gingell, D. In preparation.

CONCLUSIONS

The use of the perpendicular illumination approximation in finite aperture microscope interferometry is strongly contra-indicated. For INA between 0.76 and 1.20 (corresponding to cones of illuminating light having angles of 60° and 104°) our theory corresponds extremely closely to measured irradiances from a simple thin-film for up to ten orders of interference. In this range the theory shows that calculation of the cell-substratum gap generally depends on the cytoplasmic thickness. However for cell-substratum separations from 0–250 nm, cytoplasmic thicknesses exceeding $\sim$ 1 μm are effectively infinite if observations are made at an illuminating numerical aperture of 1.20. Under these conditions the cell-substratum model can be simplified to (glass/water/cell membrane/cytoplasm) (Fig. 14). A lamellar sheet of cytoplasm much thinner than 1 μm, however, gives rise to an appreciable error if this simplification is made, so that a separate estimation of cytoplasmic thickness is advisable where such conditions are suspected. It is not legitimate to use small illuminating apertures to avoid the difficulties associated with computing irradiances for nonperpendicular incidence, unless the thickness of the cytoplasm is known (compare curves 0.0 in Figs. 11, 12, and *b* in 14). This problem mars the interpretation of irradiances measured by Curtis (1). A further advantage of working at INA = 1.20 is that calculated irradiances are relatively insensitive to the assumed value of the membrane refractive index. We must conclude that the advantages in image interpretation at high INA outweigh the difficulties of instrumentation and computation and that there is no escape from carrying out the procedures that we have described.

It is a pleasure to thank Professor O. S. Heavens for his invaluable interest and advice. We also thank Dr. J. E. S. Bradley for discussions and particularly for his unstinting efforts in streamlining our computer program. We are indebted to Mr. R. Setterington of Carl Zeiss Ltd. (West Germany) who generously extended facilities for assessment of optical components, and to Mr. J. Knight of Oriel Scientific Ltd. for advice on light sources.

We are grateful to the Science Research Council for supporting this work.

Received for publication 16 August 1978.

REFERENCES

1. CURTIS, A. S. G. 1964. The mechanism of adhesion of cells to glass, a study by interference reflection microscopy. *J. Cell. Biol.* **20**:199.
2. ABERCROMBIE, M., and G. A. DUNN. 1975. Adhesions of fibroblasts to substratum during contact inhibition observed by interference reflection microscopy. *Exp. Cell. Res.* **92**:57.
3. IZZARD, C. A., and LINDA R. LOCHNER. 1976. Cell to substrate contacts in living fibroblasts: an interference reflexion study with an evaluation of the technique. *J. Cell. Sci.* **21**:129.
4. HEATH, J. P., and G. A. DUNN. 1978. Cell to substratum contacts of chick fibroblasts and their relation to the microfilament system. A correlated interference-reflexion and high voltage electron microscope study. *J. Cell. Sci.* **29**:197.
5. REES, D. A., C. W. LLOYD, and D. THOM. 1977. Control of grip and stick in cell adhesion through lateral relationships of membrane glycoproteins. *Nature (Lond.).* **267**:124.
6. PRESTON, T. M., and C. A. KING. 1978. Cell-substrate associations during amoeboid locomotion of *Naegleria*. *J. Gen. Microbiol.* **104**:347.
7. GINGELL, D., I. TODD, and V. A. PARSEGIAN. 1977. Long range attraction between red cells and a hydrocarbon surface. *Nature (Lond.).* **268**:767.
8. GINGELL, D., and S. VINCE. 1979. Long-range forces and adhesion: an analysis of cell-substratum studies. *In*

Adhesion and Motility of Cells. A. S. G. Curtis, editor. British Society of Cell Biology, series 3. Cambridge University Press.

9. CHERRY, R. J., and D. CHAPMAN. 1969. Optical properties of black lipid films. *J. Mol. Biol.* **40**:19.
10. Tables of dielectric data for pure ligands and dilute solutions. 1958. National Bureau of Standards, Washington, D.C. Circular 589.
11. WALLACH, D. F. H., V. B. KAMAT, and M. GAIL. 1966. Physicochemical differences between fragments of plasma membrane and endoplasmic reticulum. *J. Cell. Biol.* **30**:601.
12. LENEVEU, D. M., R. P. RAND, D. GINGELL, and V. A. PARSEGIAN. 1976. Apparent modification of forces between lecithin bilayers. *Science (Wash. D. C.).* **191**:399.